Journal of Modern Optics
Vol. 55, Nos. 19–20, 10–20 November 2008, 3305–3317

Taylor & Francis
Taylor & Francis Group

Mid/far-infrared photodetectors based on quantum coherence in coupled quantum wells

Aleksander K. Wójcik[a]*, Feng Xie[a], V.R. Chaganti[a], Alexey Belyanin[a] and Junichiro Kono[b]

[a]*Department of Physics, Texas A&M University, College Station, TX, USA;* [b]*Department of Electrical and Computer Engineering, Rice University, Houston, TX, USA*

(*Received 4 March 2008; final version received 16 July 2008*)

We propose mid/far-infrared photodetectors based on coherent sum-frequency generation in a near-resonant cascade of interband and intersubband transitions in high optical nonlinearity asymmetric quantum well structures. Such structures can yield high detectivity and responsivity in the bandwidth of the order of 30% of a central frequency in the mid-infrared range. Resonant up-conversion detectors can be designed for both collinear and perpendicular pump and signal beams. They can be integrated with semiconductor pump lasers to yield compact devices. We present specific device designs based on GaAs/AlGaAs and InGaAs/AlInAs heterostructures and calculate their expected figures of merit.

Keywords: infrared; photodetector; frequency up-conversion; coupled quantum wells; semiconductor heterostructures

1. Introduction

Existing mid/far-infrared (IR) semiconductor photodetectors demonstrate excellent, nearly background-limited performance at low temperatures, yet at non-cryogenic temperatures they suffer from high dark current due to thermal excitations across a low-energy interband, intersubband, or impurity transition. Cryogenic cooling is usually required for high detectivity, and the single-photon counting regime is not achievable. Morever, even at low temperatures an exponentially raising background limits the long-wavelength detectors performance much more severely when compared to their near-IR counterparts. These are fundamental limitations that seem to be inherent to any direct-detection technique. An alternative detection scheme is based on coherent frequency up-conversion into the near-IR/visible range by using a suitable nonlinear optical interaction [1,2]. This approach allows one to employ superior visible/near-IR detectors: avalanche photodiodes (APDs) and photomultipliers, that have low dark counts and background noise and operate at room temperature in the single-photon counting regime. Under the optimal conditions, the detectivity of up-conversion schemes is determined by the detectivity of APDs, which is several orders of magnitude higher than that of the

*Corresponding author. Email: awojcik@physics.tamu.edu

ISSN 0950–0340 print/ISSN 1362–3044 online

DOI: 10.1080/09500340802357315
http://www.informaworld.com

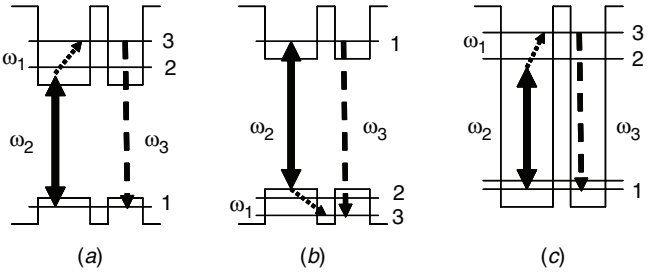

Figure 1. A sketch of near-resonant SFG employing a cascade of interband and intersubband transitions ((*a*) and (*b*)) or intersubband transitions only (*c*). Bold solid line: a near-IR pump laser at frequency ω_2; dotted line: a mid/far-infrared signal at frequency ω_1; dashed line: an up-converted radiation at frequency $\omega_3 = \omega_1 + \omega_2$.

state-of-the-art semiconductor mid-infrared detectors. Efficient up-conversion from telecom wavelengths 1.3–1.55 μm into the operating range of silicon APDs has been achieved [3,4]. Mid-infrared single-photon counting using sum-frequency generation in a periodically poled lithium niobate crystal and a silicon APD has been recently reported by Temporão et al. [5].

The nonlinear up-conversion detection has the potential to overcome the above two fundamental limitations, but unfortunately it encounters its own problem: the efficiency of nonlinear up-conversion of weak signals is low, especially in the continuous-wave regime. For example, the up-conversion efficiency reported by Temporão et al. [5] was of the order of 10^{-6}. It can be improved by employing high-power pulsed pump lasers, but the resulting system becomes bulky and inconvenient. It is known that the optical nonlinearity becomes strongly enhanced in resonant cascade schemes when all interacting fields are resonant with corresponding optical transitions in a medium and all transitions are dipole allowed. The latter condition is usually difficult to satisfy; nevertheless, such detection schemes based on resonant excitation of quantum coherence in atomic vapors have been proposed [6]. However, all practical up-conversion detector designs that could be potentially integrated with a pump source and other optoelectronic components require the use of solid-state nonlinear materials, preferably semiconductors.

In this paper we propose and theoretically analyze various detection schemes of mid/far-IR radiation by frequency up-conversion into the near-IR range via resonantly enhanced sum-frequency generation (SFG) in coupled semiconductor quantum-well structures. The schemes utilize a near-resonant cascade of interband and intersubband transitions. A near-IR laser pump, slightly detuned from the interband transition, is mixed with a mid/far-IR signal resonant to the intersubband transition in the same structure, generating near-IR sum-frequency radiation. A generic scheme of such a process is shown in Figures 1(*a*) and (*b*). For the sake of completeness, in Figure 1(*c*) we also sketch a variant of the SFG process in a resonant three-level scheme utilizing only intersubband transitions in a high band-offset heterostructure. In the present paper we will focus only on the first two schemes while the last configuration will be analyzed in detail elsewhere. The schemes offer an enhanced up-conversion efficiency at reasonable pump powers in a very compact setup that can be potentially monolithically integrated with a diode pump laser, which would yield an injection-pumped device.

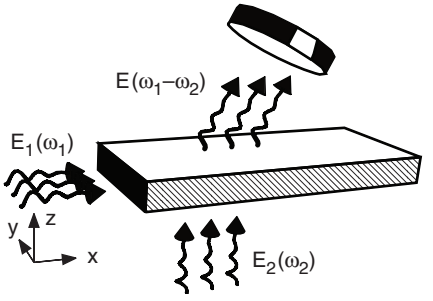

Figure 2. A sketch of the up-conversion photodetection with orthogonal pump and input signal beams.

We present some specific structures and device designs and analyze the expected performance of such detectors. We show that these devices can yield high nonlinearity and high detectivity in a spectral range of the order of 30–40 meV in the mid-infrared range, determined by the frequency dependence of resonant second-order optical nonlinearity $\chi^{(2)}$. Spectral tunability and control over spontaneous recombination noise can be achieved by applying bias and/or by tuning the pump laser. Up-conversion detectors can be designed for both collinear and perpendicular pump and signal beams. The crossed beam geometry sketched in Figure 2, valid for intersubband–interband configurations from Figures 1(*a*) and (*b*), is particularly convenient as it guarantees automatic phase matching and the up-converted signal propagates in a different direction than the pump laser beam.

Note that in this paper we do not consider the process of electron excitation by sequential absorption of two photons, followed by spontaneous interband recombination, as proposed, for example, in [7], or the integration of quantum well infrared photodetectors (QWIPs) with light-emitting diodes [8,9]. Only coherent nonlinear optical mixing is considered here. Of course, as the interacting optical fields approach resonance with interband or intersubband transitions, the SFG process is inevitably accompanied by photon absorption and emission leading to a change in electron populations. These effects could be detrimental to the photodetection scheme analyzed here as they tend to reduce detectivity by generating spontaneous emission at the sum-frequency in the absence of an input signal. Their contribution can be controlled by adjusting the pump laser intensity and detuning, as discussed below.

2. Optical nonlinearity

Resonant second-order optical susceptibility $\chi^{(2)}$ associated with intersubband and/or interband transitions in coupled quantum wells (QWs) has been calculated many times in the past; see e.g. [10] and references therein, or [11,12]. Assuming for definiteness the SFG scheme shown in Figure 1(*a*) and strictly vertical optical transitions, the main double-resonant contribution to $\chi^{(2)}$ can be estimated by solving density matrix equations as

$$\chi^{(2)} = \frac{1}{2\pi L}\int \mathrm{d}k_{\parallel}^2 \frac{\mu_{13}\mu_{23}\mu_{12}}{E_{31}(k_{\parallel}) - \hbar\omega_3 - i\gamma_{13}}\left[\frac{f_v(k_{\parallel}) - f_{c1}(k_{\parallel})}{E_{21}(k_{\parallel}) - \hbar\omega_2 - i\gamma_{12}} - \frac{f_{c1}(k_{\parallel}) - f_{c2}(k_{\parallel})}{E_{32}(k_{\parallel}) - \hbar\omega_1 - i\gamma_{23}}\right]. \quad (1)$$

Here L is a thickness of one period of the structure, γ_{ij} are the relaxation rates for the corresponding off-diagonal density matrix elements ρ_{ij}, μ_{ij} and $E_{ij}(k_\parallel)$ are the dipole matrix elements and energies of the corresponding transitions i–j for a given parallel momentum $k_\parallel$ of an electron, and $f_{v,c1,c2}$ are electron occupation numbers of relevant subbands in the valence band and in the conduction band (states 1, 2, and 3 in Figure 1(*a*)) for a given $k_\parallel$.

In general, both the dipole moments and relaxation rates depend on $k_\parallel$, and conduction band subbands are non-parabolic. These effects can be easily taken into account numerically; however, we will neglect them here for the purpose of obtaining simple analytic estimations. Furthermore, we will assume that the structure is undoped and neglect the effect of photoexcited conduction band electrons on $\chi^{(2)}$ by putting $f_v = 1$ and $f_{c1,2} = 0$.

For parabolic energy subbands of the same conduction band effective mass m_e, the interband transition energies are simply

$$E_{21}(k_\parallel) = E_{21}(0) + \frac{\hbar^2 k_\parallel^2}{2m_e} + \frac{\hbar^2 k_\parallel^2}{2m_h} = E_{21}(0) + \frac{\hbar^2 k_\parallel^2}{2m_r} \tag{2}$$

and

$$E_{31}(k_\parallel) = E_{31}(0) + \frac{\hbar^2 k_\parallel^2}{2m_r}, \tag{3}$$

where

$$\frac{1}{m_r} = \frac{1}{m_e} + \frac{1}{m_h}. \tag{4}$$

Then the integration can be easily carried out, yielding

$$\chi^{(2)} = \frac{m_r \mu_{12}\mu_{13}\mu_{23} I}{\pi\hbar^2 L} \tag{5}$$

where I is defined by

$$I \equiv \frac{1}{\delta_{12} - \delta_{13} - i(\gamma_{12} - \gamma_{13})}\left[\frac{1}{2}\ln\frac{\delta_{12}^2 + \gamma_{12}^2}{\delta_{13}^2 + \gamma_{13}^2} + i\arctan\frac{\delta_{12}}{\gamma_{12}} - i\arctan\frac{\delta_{13}}{\gamma_{13}}\right]. \tag{6}$$

Here we introduced two detuning parameters $E_{31}(0) - \hbar\omega_3 = \delta_{13}$, $E_{21}(0) - \hbar\omega_2 = \delta_{12}$.

Equation (5) contains the factor equal to the joint density of states which is defined as

$$\mathrm{d}n = \frac{m}{\pi\hbar^2 L}\mathrm{d}E \equiv \frac{\partial n}{\partial E}\mathrm{d}E. \tag{7}$$

This allows us to rewrite Equation (5) in a more intuitive form:

$$\chi^{(2)} = \frac{\partial n}{\partial E}\hbar\gamma_{12}\frac{I}{\hbar\gamma_{12}}\mu_{12}\mu_{13}\mu_{23}. \tag{8}$$

Apart from the different spectral broadening factor I, expression (8) looks similar to the second-order susceptibility of a three-level medium with an effective ground-state density $N_{eff} = (\partial n/\partial E)\hbar\gamma_{12}$ equal to the volume density of electron-hole states in the energy interval $\hbar\gamma_{12} \sim 10\,\mathrm{meV}$. For GaAs-based and InP-based heterostructures, $N_{eff}L \sim 10^{11}\,\mathrm{cm}^{-2}$.

The factor $|I|^2$ determines the spectral shape of $|\chi^{(2)}|^2$ and ultimately the spectral response of the up-conversion photodetector. Figure 3 shows an example of the $|\chi^{(2)}|^2$ dependence on detuning δ_{13} when the pump laser is detuned by $\delta_{12} = 20$ meV below the absorption band edge $E_{21}(0)$. All numerical values are chosen for a double QW InGaAs/AlInAs heterostructure lattice matched to InP, with all line broadenings γ (half-widths at half-maximum) equal to 10 meV and the product of three dipole moments equal to 280 Å^3 (see Figure 3). The intersubband transition energy is around 100 meV (12 μm wavelength). As is clear from the figure, the full-width at half-maximum of the spectral response of the detector is about 40 meV, i.e. about one-third of the mid-infrared signal frequency.

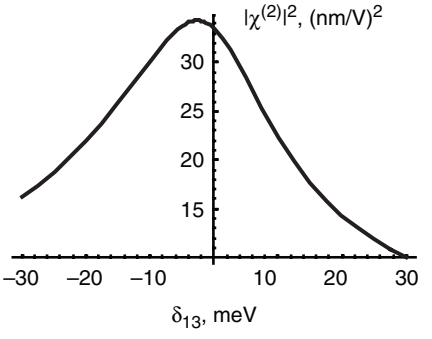

Figure 3. The value of $|\chi^{(2)}|^2$ as a function of detuning of the up-converted signal frequency from the transition 1–3. All parameters are specified in the text.

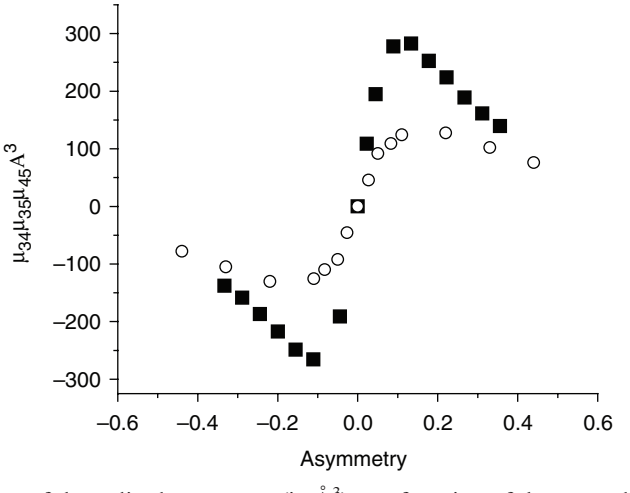

Figure 4. The product of three dipole moments (in Å^3) as a function of the normalized asymmetry of a double QW, defined as $(d_1 - d_2)/(d_1 + d_2 + d_3)$, where $d_{1,3}$ are the thicknesses of the two QWs and d_2 is the thickness of the barrier in between. Solid squares: InGaAs/AlInAs heterostructure lattice matched to InP; open circles: GaAs/$Al_{0.3}Ga_{0.7}As$ heterostructure. Graphs are plotted for a constant $d_1 + d_2 + d_3 = 90$ Å and $d_2 = 10$ Å.

Tuning the pump laser closer to the band gap increases the maximum nonlinearity but also increases the pump absorption, which leads to enhanced spontaneous recombination of photoexcited electrons and ultimately to higher noise-equivalent power and lower detectivity. One should choose an optimal pump detuning depending on the specific application.

For a given detuning, the strength of the nonlinearity is characterized by the product of three dipole moments $\mu_{12}\mu_{13}\mu_{23}$. To obtain a large value of the product one needs to use asymmetric heterostructures. A vast number of different configurations have been proposed in the literature: step QWs, double, triple, biased QWs, etc. We have performed $k \cdot p$ simulations in various approximations (from eight-band to an effective three-band) for a large number of QW configurations and found that for a given material system and given intersubband transition energy the maximum values of the above product in the unbiased QWs are similar within a factor of two. In Figures 4–6 we show the simulation results for an unbiased double QW for two heterostructures: the InGaAs/AlInAs heterostructure lattice matched to InP and the $GaAs/Al_{0.3}Ga_{0.7}As$ heterostructure. They illustrate optimal QW thicknesses and asymmetry and maximum nonlinearity achieved in these heterostructures for various intersubband transition energies in the mid/far-infrared range. Peak responsivity of the detector is reached at the photon energy of the signal roughly equal to the intersubband transition energy. Maximum values of $|\chi^{(2)}|$ in the mid-infrared range at 10 μm wavelength are within 5–20 nm/V. Applying an optimal bias leads to an increase in $|\chi^{(2)}|$ by a factor of two to four as compared to the peak values in Figure 4. Figure 7 shows the change in the product of three dipole moments

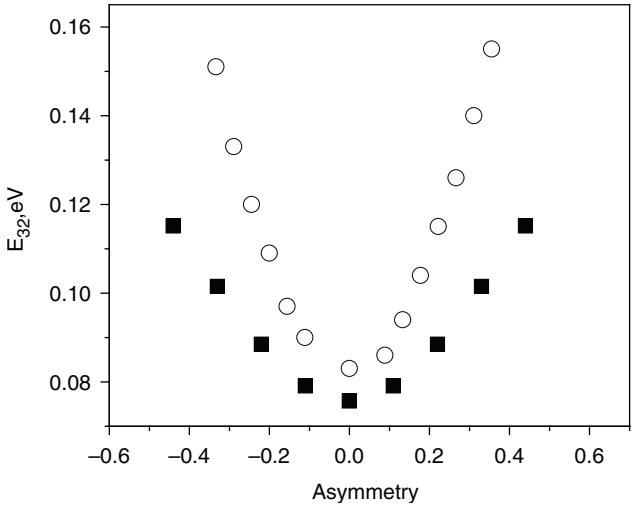

Figure 5. The intersubband transition energy as a function of the normalized asymmetry of a double QW, defined as $(d_1 - d_2)/(d_1 + d_2 + d_3)$, where $d_{1,3}$ are the thicknesses of the two QWs and d_2 is the thickness of the barrier in between. Solid squares: InGaAs/AlInAs heterostructure lattice matched to InP; open circles: $GaAs/Al_{0.3}Ga_{0.7}$ As heterostructure. Graphs are plotted for a constant $d_1 + d_2 + d_3 = 90$ Å and $d_2 = 10$ Å.

with applied electric field for a double GaAs/$Al_{0.3}Ga_{0.7}As$ QW of the same total thickness of 90 Å.

The nonlinearity in InGaAs/AlInAs heterostructures is stronger by a factor of two to three as compared to GaAs/AlGaAs system. However, because of a narrower band gap of InGaAs the wavelengths of the up-converted signal are typically in the range 1.1–1.2 μm.

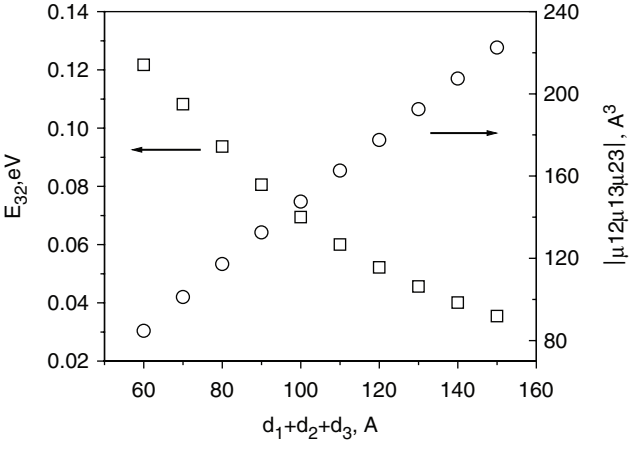

Figure 6. The intersubband transition energy (squares, left axis) and the product of three dipole moments (circles, right axis) as functions of the total thickness $d_1 + d_2 + d_3$ of a double GaAs/$Al_{0.3}Ga_{0.7}As$ QW, where $d_{1,3}$ are the thicknesses of the two QWs and d_2 is the thickness of the barrier in between. Graphs are plotted for a constant asymmetry ratio $(d_1 - d_2)/(d_1 + d_2 + d_3) = 0.2$ and $d_2 = 10$ Å.

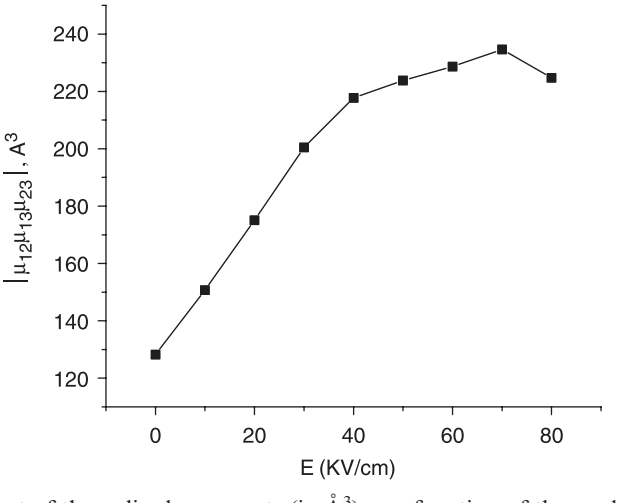

Figure 7. The product of three dipole moments (in $Å^3$) as a function of the applied external electric field for a double GaAs/$Al_{0.3}Ga_{0.7}As$ QW heterostructure consisting of 30 and 50 Å wells separated by a 10 Å barrier.

For detection in this range one has to use InGaAs APDs that have lower efficiency as compared to silicon APDs. In GaAs-based heterostructures the up-converted signal does fit into the operating range of superior silicon APDs. This can be an important advantage for low signal detection and single-photon counting.

The relaxation time of the nonlinear polarization is very fast, of the order of 0.1–1 ps. Therefore, the up-conversion process does not limit the dynamic response time of the proposed detector. The dynamic response of the overall detection system is limited by the near-IR APD, which is usually in the nanosecond range.

3. Detector geometry and up-conversion efficiency

The detector geometry and beam alignment depend on which of the up-conversion schemes in Figure 1 we choose. For the scheme in Figure 1(*a*), the mid/far-infrared signal should have a transverse magnetic (TM)-polarization and come from the facet, while the near-IR pump can either come from the facet or propagate at normal incidence to the layers as shown in Figure 2. For the scheme in Figure 1(*b*) one has an additional opportunity of both signal and pump having TE polarization and propagating normal to the layers if the transition 2–3 occurs between the first heavy-hole and second light-hole subbands. In this case, maximum nonlinearity is lower by a factor of seven to eight as compared to using a TM-polarized intersubband transition. However, in some cases, it may be worth sacrificing the nonlinearity for a simpler normal incidence geometry. Finally, for the scheme in Figure 1(*c*) all beams should have TM-polarization.

Here we will consider only the crossed beam configuration sketched in Figure 2 and shown in Figure 8 in more detail. For the input mid-infrared signal field E_1 and the near-IR pump E_2 we can write

$$\begin{aligned} \mathbf{E_1} &= \left(A_1(z)e^{ik_1 x}e^{-i\omega_1 t} + \text{c.c.}\right)\hat{x}, \\ \mathbf{E_2} &= \left(A_2(x)e^{ik_2 z}e^{-i\omega_2 t} + \text{c.c.}\right)\hat{y}, \end{aligned} \tag{9}$$

where the hat over a variable denotes a unit vector and c.c. represents complex conjugate. The fields will interact in the active region (a stack of many periods of double QWs) generating a sum-frequency field of the form

$$\mathbf{E} = \left(A(x,z)e^{i\mathbf{k}\cdot\mathbf{r}}e^{-i\omega t} + \text{c.c.}\right)\hat{y} \tag{10}$$

which propagates in the (x,z)-plane along the phase-matched direction specified below. We will drop the subscript 3 in the variables and parameters related to the up-converted field. In order to simplify the problem, we assume that the fields do not depend on y. Under those assumptions, the equation for the output field becomes

$$\nabla^2 E + \frac{\omega^2 \varepsilon}{c^2} E = \frac{-4\pi\omega^2}{c^2}\chi^{(2)} E_1 E_2. \tag{11}$$

We will assume that the dielectric constant in the active region is a weighted average of dielectric constants of individual layers. In the slow-varying amplitude approximation and

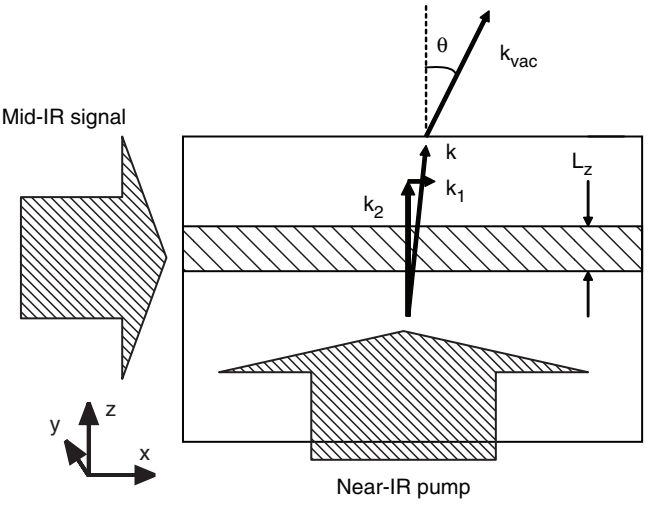

Figure 8. SFG geometry with crossed pump and input signal beams. L_z is the total thickness of the multiple QW active region. The up-converted signal propagates in the phase-matched direction k determined by $k_x = k_1$.

assuming that no appreciable depletion of input fields occurs, we have

$$2i\left(k_x \frac{\partial A}{\partial x} + k_z \frac{\partial A}{\partial z}\right) e^{i\mathbf{k}\cdot\mathbf{r}} = \frac{-4\pi\omega^2}{c^2} \chi^{(2)} E_1 E_2. \tag{12}$$

We solve this equation by making a suitable change of variables [13],

$$\begin{bmatrix} \eta \\ \xi \end{bmatrix} = \frac{1}{k} \begin{bmatrix} k_x & k_z \\ -k_z & k_x \end{bmatrix} \begin{bmatrix} x \\ z \end{bmatrix}, \tag{13}$$

$$\begin{bmatrix} x \\ z \end{bmatrix} = \frac{1}{k} \begin{bmatrix} k_x & -k_z \\ k_z & k_x \end{bmatrix} \begin{bmatrix} \eta \\ \xi \end{bmatrix}. \tag{14}$$

The new variables represent a new orthogonal coordinate system, where $\hat{\eta}$ is in the same direction as $\mathbf{k}$, while $\hat{\xi}$ is orthogonal to it. This transformation reduces the number of independent variables to one:

$$k \frac{\partial A}{\partial \eta} = \frac{\partial A}{\partial x} k_x + \frac{\partial A}{\partial z} k_z. \tag{15}$$

This allows us to find a general solution to Equation (12),

$$A(\eta, \xi) = \frac{2\pi i \omega^2}{c^2} \int_0^{\eta} \chi^{(2)} E_1(\eta', \xi) E_2(\eta', \xi) e^{-i\mathbf{k}\cdot\mathbf{r}} \, \mathrm{d}\eta' + g(\xi), \tag{16}$$

where g is an arbitrary function of ξ, chosen to satisfy the geometry-dependent boundary conditions. Note that $\chi^{(2)}$ is assumed to be non-zero only in the active region.

We proceed by defining phase-mismatching parameters in the standard way:

$$\Delta k_x = k_1 - k_x; \quad \Delta k_z = k_2 - k_z, \quad \Delta\mathbf{k} = \Delta k_x \hat{x} + \Delta k_z \hat{z}.$$

Since the interaction region is thin in the z-direction, we can approximate the amplitudes of the input fields by constants inside it, which gives us an exact solution for the integral:

$$\begin{aligned} A(\eta,\xi) &= \frac{2\pi i\omega^2}{c^2} A_1 A_2 \int_0^\eta \chi^{(2)} e^{i(k_1 x + k_2 z)} e^{-i\mathbf{k}\cdot\mathbf{r}}\, \mathrm{d}\eta' + g(\xi) \\ &= \frac{2\pi i\omega^2}{c^2} A_1 A_2 \int_0^\eta \chi^{(2)} e^{i\Delta\mathbf{k}\cdot\mathbf{r}}\, \mathrm{d}\eta' + g(\xi). \end{aligned} \tag{17}$$

Evaluating the integral gives

$$A = \frac{2\pi i\omega^2}{kc^2}\chi^{(2)} \frac{A_1 A_2}{i\Delta\mathbf{k}\cdot\mathbf{r}|_{\eta=1,\xi=0}} \left[e^{i\Delta\mathbf{k}\cdot\mathbf{r}} - e^{i\Delta\mathbf{k}\cdot\mathbf{r}|_{z=0}}\right], \tag{18}$$

where the last term comes from our particular boundary condition

$$A(x, z=0) = 0. \tag{19}$$

This means that the up-converted field has zero amplitude at the lower boundary of the active region. The final expression for the amplitude, presented in the original coordinate system, is

$$A(x,z) = \frac{2\pi\omega^2}{c^2}\chi^{(2)} A_1 A_2 \frac{\left(e^{i\Delta\mathbf{k}\cdot\mathbf{r}} - e^{i\Delta k_x x}\right)}{(\Delta k_x k_x + \Delta k_z k_z)}. \tag{20}$$

Since the refractive index grows with frequency, the value of $|\mathbf{k}|$ is greater than $|\mathbf{k_1} + \mathbf{k_2}|$ for any direction of $\mathbf{k}$. However, phase matching is still possible if the active region thickness L_z is small enough so that

$$\Delta k_z L_z \ll 1. \tag{21}$$

In this case the phase-matched direction will be determined by $\Delta k_x = k_1 - k_x = 0$ (see Figure 8). Under the last two conditions, Equation (20) reduces to

$$A(x, L_z) = \frac{2\pi i\omega^2}{c^2}\chi^{(2)} A_1 A_2 \frac{L_z}{k_z}. \tag{22}$$

The condition (21) is violated when L_z becomes larger than a few micrometers, which is not very restrictive. In any case the value of L_z should be limited by absorption of the pump and an up-converted signal to about a hundred QW periods, which is of the order of 1–2 μm. Therefore, phase-matched generation is guaranteed in this geometry.

The angle between vectors $\mathbf{k}$ and $\mathbf{k_2}$ is of the order of k_1/k_2, i.e. about 5–10 degrees in the mid-IR range. After refraction at the boundary between the semiconductor and air this angle increases to $\theta \sim$20–40 degrees. This separates the directions of the strong pump and weak up-converted signal, which is another important advantage of this geometry.

The total output SFG power in the phase-matched direction is

$$P = \frac{2\pi n\omega^4}{c^3}\frac{|\chi^{(2)}|^2(A_1A_2)^2L_z^2L_x}{k_z^2}, \tag{23}$$

where L_x is the length of the pumped spot in the x-direction. Assuming that the mid-infrared signal has overlap Γ with the active region in the z-direction, and the pump and the signal are overlapped over the length L_y in y-direction, Equation (23) can be expressed through the total signal power P_1 and the pump intensity in the mixing region I_2 as

$$P \simeq \frac{4\pi^3\omega^2}{c^3nn_1n_2}|\chi^{(2)}|^2L_zL_x\Gamma I_2P_1, \tag{24}$$

where n, n_1, n_2 are the refractive indices of the three interacting beams in the active region. Note that the mid-IR radiation can be guided in the crystal, in which case n_1 is an effective modal refractive index. The power up-conversion efficiency defined as $\eta_{up} = P/P_1$ is an important figure of merit of the detector.

4. Detector performance

Although the proposed mid/far-infrared photodetection scheme consists of two steps, up-conversion and subsequent detection by a near-IR APD, it can be still characterized by standard figures of merit: the noise equivalent power (NEP), which is inversely proportional to the detectivity, the quantum efficiency, and the responsivity. The intrinsic noise of our detector in the absence of an input signal has several contributions: an intrinsic noise of the near-IR APD, background radiation at the sum-frequency, background noise at the mid-IR signal frequency up-converted by SFG process, and spontaneous recombination emission of the QW structure in the absence of a signal. Ideally, we would like to have all contributions below or comparable to the intrinsic APD noise. In this case the detectivity of the whole scheme is determined by the detectivity of the near-IR APD. The up-converted background noise is mostly filtered out by the phase-matched SFG process since only one spatial mode of this noise can be up-converted efficiently. Spontaneous emission at frequencies near the sum-frequency ω from the multiple QW (MQW) structure is due to excitation of electrons and holes by a strong pump, followed by radiative recombination of a hot tail of the distributions of photoexcited carriers having parallel momenta $k_\parallel$ satisfying the condition

$$\hbar\omega = E_{21}(0) + \frac{\hbar^2k_\parallel^2}{2m_r}. \tag{25}$$

The noise signal power reaching the detector within the frequency bandwidth $\Delta\omega$ and a solid-angle aperture $\Delta\Omega \ll 1$ of the detector, which is set to receive only a highly collimated sum-frequency signal, can be estimated as

$$P_{sp} = A(k_\parallel)n_e(k_\parallel)n_h(k_\parallel)V_{MQW}\Delta\omega\frac{\Delta\Omega}{4\pi}, \tag{26}$$

where A is the spectral density of the spontaneous emission rate and V_{MQW} the pumped volume of the active region. The density of hot electrons and holes with a given parallel

momentum obeys the Boltzmann distribution in the simplest case. It can be calculated from the absorbed power of the pump radiation and can be controlled by the detuning δ_{12} of the pump below the band edge and by the pump intensity I_2.

Recent advances have pushed the NEP of APDs to very low values of $10^{-15}\,\mathrm{W/cm^{1/2}}$ even for InGaAs APDs at room temperatures [14]. Ideally, we would like P_{sp} to be below the NEP of the near-IR APD, which limits the pump intensity I_2 to about $10^6\,\mathrm{W/cm^2}$ for $E_{32} \sim 100\,\mathrm{meV}$, $\Delta\Omega \sim 0.01$, $\delta_{12} \sim 30\,\mathrm{meV}$, and reasonable values of all other parameters. Note that the spontaneous recombination radiation is external for an APD. Therefore, even if P_{sp} is higher than the APD's NEP, its effect on the overall detectivity of a system can be reduced by subtracting the APD readings in the presence and the absence of the input mid-IR signal.

Under the above optimal condition of low optical population transfer the up-conversion process is almost insensitive to temperature since thermal excitation across the band gap is negligible. The only temperature dependence of $\chi^{(2)}$ may come from the dephasing rates γ_{ij} that do not show strong temperature variation because they are usually dominated by interface roughness. Therefore, the temperature sensitivity of the overall detection system is determined by the near-IR APD.

Another kind of noise specific to the up-conversion detection is due to the fact that the output sum-frequency signal is effectively modulated by the pump laser intensity. The pump laser can have intensity fluctuations, a kind of noise known as relative intensity noise (RIN) [15]. This noise will introduce small fluctuations in the output power, proportional to the intensity of the signal. This noise can be neglected for NEP calculations, but it can introduce a certain noise level depending on the specific system.

The overall photon conversion efficiency is given by

$$\eta = \frac{\omega_1}{\omega}\eta_{up}\eta_c\eta_{APD}, \tag{27}$$

where $\eta_{up} = P/P_1$, η_c is the coupling efficiency of the sum-frequency radiation to the APD which can be close to 1, and η_{APD} is the detection efficiency of the APD. For the structures considered in Section 1 and the pump intensity $I_2 \sim 10^6\,\mathrm{W/cm^2}$, we obtain η of the order of 0.1%. The primary reason for low efficiency is a short interaction length L_z of the order of $1\,\mu\mathrm{m}$. The efficiency can much higher for collinear guided in-plane propagation of the signal and pump beams. In this case the sum-frequency radiation propagates in a phase-matched direction $k_x = k_1 + k_2$ at a small angle ~5–10 degrees to the waveguide axis. After refraction on the cavity facet it propagates at a much larger angle of 20–30 degrees with respect to the waveguide axis, ensuring separation of the pump and the up-converted signal in space. However, a larger detuning of the pump from the interband transition is needed in this case. We consider this geometry elsewhere.

The overall responsivity defined as the ratio of the APD photocurrent to the mid-IR signal power P_1 incident on a crystal is given by

$$R = \frac{I_{APD}}{P_1} = \eta_{up}\eta_c R_{APD}, \tag{28}$$

where R_{APD} is the APD responsivity.

In conclusion, the proposed mid/far-IR photodetection scheme has the potential of reaching very high room-temperature detectivity values comparable to that of

state-of-the-art near-IR APDs. There is a trade-off between the detectivity and photon conversion efficiency which originates from spontaneous emission by carriers generated in QWs by a strong pump.

Acknowledgements

This work was supported in part by NSF Grants ECS-0547019 (CAREER), EEC-0540832 (MIRTHE ERC), and OISE 0530220.

References

[1] Midwinter *J. Appl. Phys. Lett.* **1968,** *12,* 68–70.
[2] Boyd, R.; Townes, C. *Appl. Phys. Lett.* **1977,** *31,* 440–442.
[3] Langrock, C.; Diamanti, E.; Roussev, R.V.; Yamamoto, Y.; Fejer, M.M.; Takesue, H. *Opt. Lett.* **2005,** *30,* 1725–1727.
[4] Thew, R.T.; Tanzilli, S.; Krainer, L.; Zeller, S.C.; Rochas, A.; Rech, I.; Cova, S.; Zbinden, H.; Gisin, N. *New J. Phys.* **2006,** *8,* 1–12.
[5] Temporão, G.; Tanzilli, S.; Hugo Zbinden, N.G.; Aellen, T.; Giovannini, M.; Faist, J. *Opt. Lett.* **2006,** *31,* 1094–1096.
[6] Boyd, R.W.; Scully, M.O. *Appl. Phys. Lett.* **2000,** *77,* 3559–3561.
[7] Vagos, P.; Boucaud, P.; Julien, F.; Lourtioz, J.M.; Planal, R. *Phys. Rev. Lett.* **1993,** *70,* 1018–1021.
[8] Ryzhii, M.V.; Ershov, M.R.; Khmyrova, I. *Jpn. J. Appl. Phys.* **1995,** *34,* L38–L40.
[9] Liu J, H.C.; Li, Z.W.; Buchanan, M. *Electron. Lett.* **1995,** *31,* 832–833.
[10] Khurgin, J. In *Nonlinear Optics in Semiconductors II*; Garmire, E., Cost, A., Eds.; Academic Press: San Diego, 1999; pp 2–83.
[11] Neogi, A.; Takahashi, Y.; Kawaguchi, H. *IEEE J. Quantum Electron.* **1996,** *32,* 701–711.
[12] Gmachl, C.; Belyanin, A.; Sivco, D.; Peabody, M.L.; Owschimikow, N.; Sergent, A.M.; Capasso, F.; Cho, A.Y. *IEEE J. Quantum Electron.* **2003,** *39,* 1345–1355.
[13] Berg, P.W.; McGregor, J.L. *Elementary Partial Differential Equations;* Holden-Day: San Francisco, 1966.
[14] Pellegrini, S.; Warburton, R.E.; Tan, L.J.J.; Ng, J.S.; Krysa, A.B.; Groom, K.; David, J.P.R.; Cova, S.; Robertson, M.J.; Buller, G.S. *IEEE J. Quantum Electron.* **2006,** *42,* 397–403.
[15] Peterman, K. *Laser Diode Modulation and Noise;* Kluwer Academic: London, 1991.